Journal of Molecular Modeling (2019) 25: 305
https://doi.org/10.1007/s00894-019-4150-0

ORIGINAL PAPER

Further understanding of the Ru-centered [2+2] cycloreversion/cycloaddition involved into the interconversion of ruthenacyclobutane using the Grubbs catalysts from a reaction force analysis

Katherine Paredes-Gil[1] · Fernando Mendizábal[2] · Pablo Jaque[3]

Received: 30 April 2019 / Accepted: 8 August 2019 / Published online: 7 September 2019

Abstract

The chemical reactivity of the first- and second-generation Grubbs catalysts has always been a significant issue in olefin metathesis. In the present work, we study the [2+2] cycloreversion/cycloaddition and the alkylidene rotation involved into the interconversion of the ruthenacyclobutane intermediate, through the reaction force and reaction force constant analysis. It has been found that the structural contribution controls the barrier energy in the interconversion of ruthenacyclobutane via [2+2] cycloreversion/cycloaddition, which is slightly lower in the second generation of Grubbs catalysts while its electronic contribution is slightly higher, which unveils a major rigidity and donor/acceptor properties of the NHC. This finding explains a greater structural contribution in the rate constant. Moreover, on the basis of the reaction force constant, the process can be classified as "two-stage"-concerted reactions, noting a more asynchronous process when the first generation is used as a catalyst.

Finally, a similar analysis into the alkylidene rotation was performed. It was determined that [2+2] cycloreversion and alkylidene rotations take place in a sequential manner, the energy barrier is again controlled by structural reorganization, and the pathway is less asynchronous.

Keywords Ru-centered [2+2] cycloreversion/cycloaddition · Reaction force constant · Grubbs catalysts · Density functional calculations

Introduction

Olefin metathesis is a rearrangement of C-C double bonds, which leads to new alkenes [1]. Currently, this process is one of the most relevant reactions in organic synthesis, since it is utilized in many industrially valuable processes, such as in the production of polymeric materials and pharmaceutical products [2–5]. This reaction occurs with a metal-carbene complex as catalyst. The molybdenum-based Schrock catalysts [6–8] and the ruthenium-based complexes, so-called Grubbs catalysts [9, 10], are the most important catalysts in this field. In general, the first- [11] and second-generation Grubbs catalysts [12, 13] are the most widely used in commercial settings. Recently, the Ru-chelated [14] and Hoveyda-catechothiolate catalysts [15] have also been shown outstanding performance (e.g., see in Fig. 1). All these proceed through the Chauvin's general mechanism [16, 17], which involves the following elementary steps: (i) the 14e- specie formation, (ii) alkene coordination (AC), (iii) [2+2] cycloaddition (CA), (iv)

This paper belongs to Topical Collection QUITEL 2018 (44th Congress of Theoretical Chemists of Latin Expression)

Electronic supplementary material The online version of this article (https://doi.org/10.1007/s00894-019-4150-0) contains supplementary material, which is available to authorized users.

✉ Katherine Paredes-Gil
k.paredesg@utem.cl

[1] Programa Institucional de Fomento a la Investigación, Desarrollo e Innovación, Universidad Tecnológica Metropolitana, Ignacio Valdivieso 2409, P.O. Box 8940577, San Joaquín, Santiago, Chile

[2] Facultad de Ciencias, Departamento de Química, Universidad de Chile, Las Palmeras 3425, Santiago, Chile

[3] Departamento de Química Orgánica y Fisicoquímica, Facultad de Ciencias Químicas y Farmacéuticas, Universidad de Chile, Sergio Livingstone 1007, Santiago, Chile

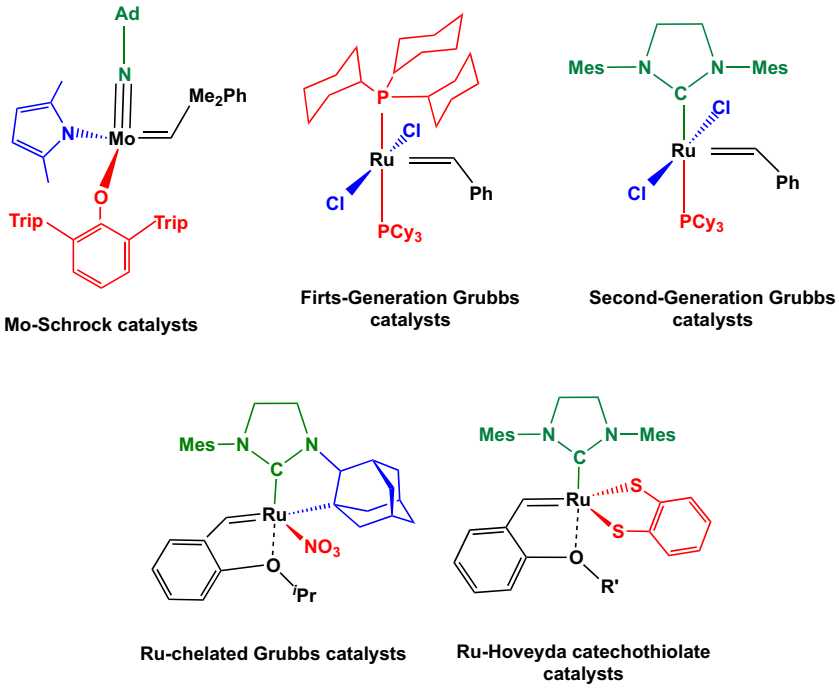

Fig. 1 The most important catalysts currently used in olefin metathesis

[2+2] cycloreversion (CR), and (v) the alkene de-coordination (AdC) (see Fig. 2).

Many experimental and computational studies have been focused on the chemical reactivity of the first- and second-generation Grubbs catalysts [18–24]. It is well-known that the latter is more catalytically efficient than the former. Kinetic studies unveiled that the phosphine dissociation is the rate-determining step ($k_1 = 9.6 \pm 0.2$ and 0.13 ± 0.01 s^{-1}; and $\Delta H_{act} = 23.6 \pm 0.5$ and 27 ± 2 kcal mol^{-1} for the first and second generation, respectively) [25–27]. A reverse *trans*-effect during this step in the second generation was also evidenced. In this context, the better performance of the second generation was explained as a consequence of the lower rotameric energy barrier [23, 28] ($\Delta E_{rota} = 13.3$ and 4.8 kcal mol^{-1} for the first and second generation, respectively) needed to transform the 14e- inactive specie into 14e- active specie. Moreover, among other important differences between these Ru-based catalysts, is the fact that the steps (ii)–(v) are much faster in the second than in the first generation ($k_{-1}/k_2 = 1.3 \times 10^4$ and 1.25 for the first and second generation, respectively) [25]. This suggests that the olefin is quickly coordinated, and thus indicating that the rotameric change could occur in its presence and moreover that the enhanced reactivity of the second-generation Grubbs catalysts in relation to the alkenes also produces a dynamic interconversion of the ruthenacyclobutane intermediate via [2+2] cycloreversion/cycloaddition [29, 30]. This is especially the case when the substituted olefins are employed. Wenzel and Grubbs, who focused their attention on this behavior, proposed thus the "olefin flips" and the "alkylidene rotation" as possible routes for

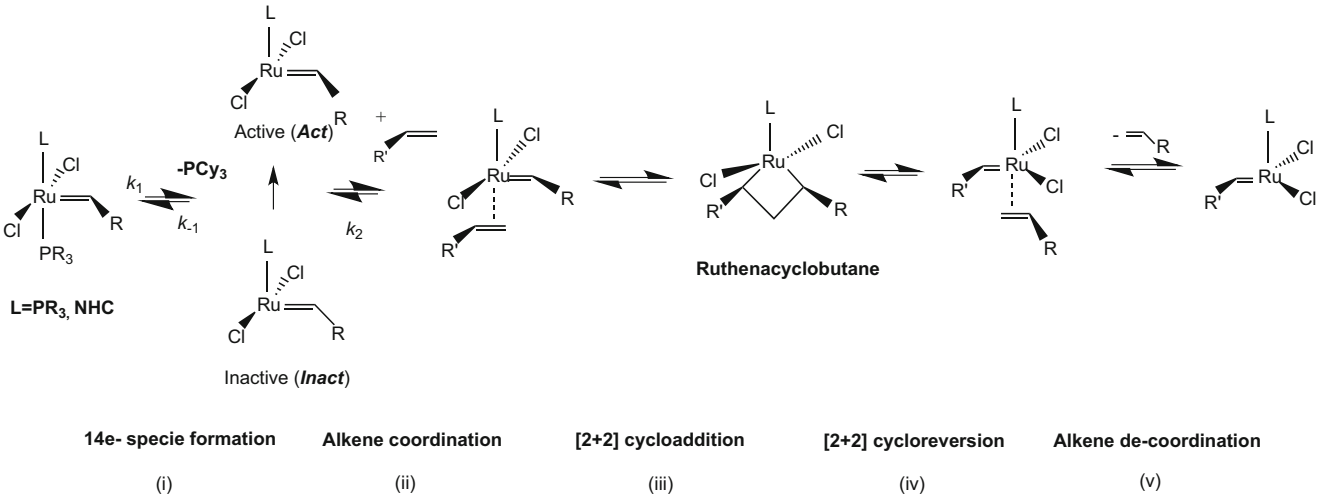

Fig. 2 Olefin metathesis mechanism proposed by Chauvin employing the first- and second-generation Grubbs catalysts

this exchange [29, 30]. Some years ago, we reported that the "alkene rotation" is the most favorable pathway for this interconversion [22]. Also, we found that in the more simple ruthenacyclobutane, formed by the reaction between the 14e-Ru-methylidene specie and ethene, the activation energies corresponding to the alkylidene rotation, alkene rotation, and [2+2] cycloaddition are alike, being consequently competitive (16.0, 13.4, and 10.6 kcal mol^{-1}, respectively) [22]. Taking into account the abovementioned facts, it is important to gain new insight into the alkylidene rotation and [2+2] cycloreversion/cycloaddition processes, employing the first- and second-generation Grubbs catalysts. This will allow a greater understanding of the chemical reactivity of these two outstanding generation Grubbs catalysts, and find new differences between them. Therefore, a new viewpoint to understand the olefin metathesis by using some interpretative tools, for instance, the reaction force/reaction force constant analysis, will be performed [31–34].

Additionally, from a mechanistic viewpoint, the Ru-centered [2+2] cycloreversion/cycloaddition reactions involve the breaking/forming of two single bonds (Ru-C and C-C) passing for the formation of two double (Ru-C and C-C) bonds character near to the transition state. In general, these can proceed in a concerted or stepwise mechanism, depending on whether the two new single bonds are formed in a single kinetic step or in two kinetic steps, respectively, with the latter involving an intermediate. The former can be further classified as synchronous or asynchronous (also called "two-stage"), depending on whether or not the new single bonds are broken/formed at the unison [35]. In this sense, these synchronicity/nonsynchronicity issues are very important in a mechanistic study in order to understand more completely the formation of the new chemical bonds in the cycloreversion/cycloaddition reactions that are involved in olefin metathesis. In order to gain a greater understanding of this issue, the reaction force constant, $\kappa(\xi)$ [33], has recently been proposed as a suitable indicator of the degree of synchronicity in multi-bond reactions [36], e.g., double-proton transfer [37, 38] and Diels-Alder reactions [39–42]. Therefore, the main goal of this work is to gain a deeper understanding of the Ru-centered [2+2] cycloaddition step involved in olefin metathesis mechanism, using the first- and second-generation Grubbs catalysts, from the reaction force perspective. Therefore, our main aim is to continue contributing to the clarification of the chemical reactivity of these two important generations because, currently, they are taken as a base identity for the future design of new catalysts.

Theoretical background

Potential energy and reaction force/reaction force constant analysis

For an elementary reaction which advances in a single kinetic step, the potential energy profile $V(\xi)$ along the minimum energy path typically computed using the intrinsic reaction coordinate (ξ) method proposed by Fukui [43] and implemented by Gonzalez and Schlegel [44] (see the top panel in Fig. 3). This can be easily obtained the activation barrier (ΔE_{act}) and the overall energy change (E°) from the energies of the stationary states, i.e., reactant (at ξ_R), transition state (at ξ_{TS}), and product (at ξ_P) as follows: $\Delta E_{act} = V(\xi_{TS}) - V(\xi_R)$ and $\Delta E^{\circ} = V(\xi_P) - V(\xi_R)$, respectively. From a mechanistic viewpoint, much valuable information can be extracted from the nonstationary states, which define the shape of both $V(\xi)$ and its derivatives.

Based on classical physics, the negative derivative and second derivative of the potential energy $V(\xi)$ define, respectively, the reaction force $\mathbf{F}(\xi)$ [31] and the reaction force constant $\kappa(\xi)$ [33] as follows:

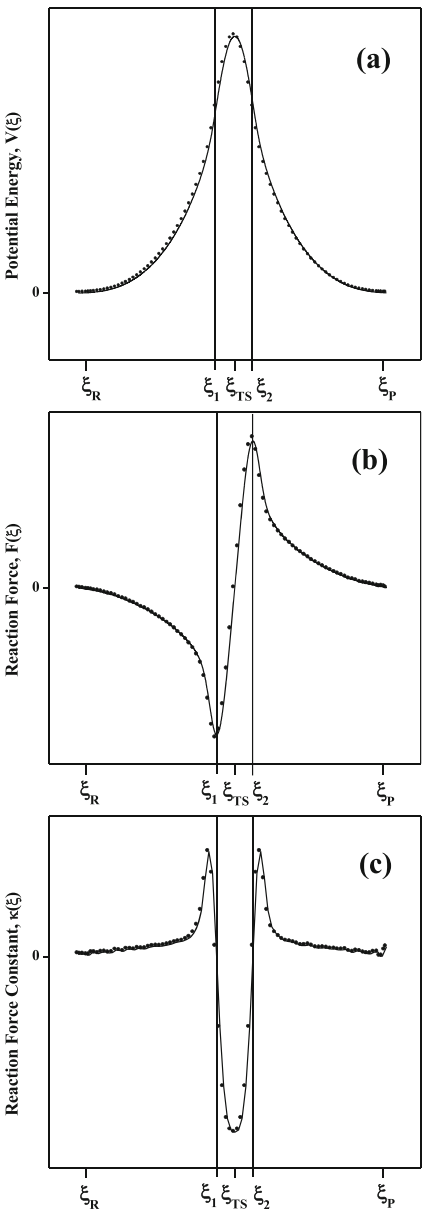

Fig. 3 Profiles of **a** $V(\xi)$, **b** $\mathbf{F}(\xi)$, and **c** $\kappa(\xi)$ along the IRC of a generic one-barrier reaction

$$F(\xi) = -\frac{\partial V(\xi)}{\partial \xi} \quad (1)$$

$$\kappa(\xi) = \frac{\partial^2 V(\xi)}{\partial \xi^2} \quad (2)$$

Both $\mathbf{F}(\xi)$ and ξ are vectors directed from reactants to products. The respective profiles of $\mathbf{F}(\xi)$ and $\kappa(\xi)$ for a single barrier $V(\xi)$ profile are shown in the middle and bottom panels in Fig. 3.

The reaction force displays typical features (see the middle panel in Fig. 3) [45–53]. It is retarding (or negative) in the region encompassed from R to TS and is driving (or positive) from TS to P, where these are equalized at the TS position. Moreover, two critical points are evidenced in the regions indicated above, a minimum (at ξ_1) and a maximum (at ξ_2), respectively. On the basis of the pattern exhibited by $\mathbf{F}(\xi)$, it has been possible to divide the chemical reaction into three meaningfully regions along ξ: the so-called "reactant" region between ξ_R and ξ_1, the "transition" region between ξ_1 and ξ_2 and finally, the "product" region between ξ_2 and ξ_P [32, 54]. In accordance with a detailed analysis of how structural and electronic properties evolve along ξ, the first and third regions are identified as structurally accentuated, since such several structural changes as rotations and bond lengthening are seen to be taking place. Meanwhile, the "transition" region is seen as an electronically accentuated one because the bond-forming/breaking are mainly encompassed throughout the transition region [53]. Although a structurally and electronically predominance is recognized in the first/third and transition regions, respectively, they are not exclusively so. This characteristic allows a partition of the energy barrier into two contributions, one associated with structural rearrangements ($\Delta E_{act,\,1}$) and the other with electronic reorganizations ($\Delta E_{act,\,2}$) as follows:

$$\begin{aligned} \Delta E_{act} &= V(\xi_{TS}) - V(\xi) \\ &= [V(\xi_1) - V(\xi_R)] + [V(\xi_{TS}) - V(\xi_1)] \\ &= \Delta E_{act,1} + \Delta E_{act,2} \end{aligned} \quad (3)$$

This framework has helped the effect of an external agent such as substituents, catalysts, or solvent on the energy barrier to be rationalized, depending on whether they affect its structural or electronic component [55, 56].

On the other hand, the reaction force constant $\kappa(\xi)$ [33] which is an energy-derived property that carries information on how the chemical bonding or interactions evolve along ξ [33] has recently been proposed as a suitable indicator of the degree of synchronicity/nonsynchronicity in concerted multi-bond chemical reactions [38–40]. The striking feature is that $\kappa(\xi)$ is negative not only with respect to the traditional TS but also throughout the whole transition region, where all bond-forming/breaking processes are encompassed. It takes positive values throughout the structurally intensive first and third regions, as shown in the bottom panel in Fig. 3. More specifically, a single minimum in $\kappa(\xi)$ is associated with a fully or nearly fully synchronous process. A significant level of asynchronicity (as a "two-stage"-concerted reaction [36]) is evidenced by a negative local maximum of $\kappa(\xi)$ connected to two $\kappa(\xi)$ minima in both sides, i.e., before leaving the transition region toward to the reactant side and the product side in the proximity at ξ_1 and ξ_2. Finally, when the maximum of $\kappa(\xi)$ becomes positive, a highly asynchronous process can transition into a stepwise mechanism with a metastable intermediate [34].

All the abovementioned has been widely discussed in Diels-Alder cycloadditions [39–42], double-proton transfer [38], water-assisted proton transfer [37], among others [34], thereby demonstrating the usefulness of both $\mathbf{F}(\xi)$ and $\kappa(\xi)$ concepts as interpretative tools in chemical reactivity studies.

Kinetic aspects

Assuming an Arrhenius model for the rate constant k of a process with activation energy, ΔE_{act}, and considering its partition into two components, $\Delta E_{\mathrm{act},\,1}$ and $\Delta E_{\mathrm{act},\,2}$ (the former a structural and the latter an electronic contribution to the activation energy), k can thus also be partitioned into two contributions, called as k_{struct} and k_{electr}:

$$\begin{aligned} k &= \mathrm{A}e^{-\Delta E_{\mathrm{act}}/\mathrm{RT}} \\ &= \mathrm{A}e^{-\Delta E_{\mathrm{act},1}/\mathrm{RT}} \cdot e^{-\Delta E_{\mathrm{act},2}/\mathrm{RT}} = k_{\mathrm{struct}} \cdot k_{\mathrm{electr}} \end{aligned} \quad (4)$$

where A is the Arrhenius factor, R is the gas constant, and T is the temperature.

Computational details

All calculations have been performed within the density functional theory (DFT) framework using the GAUSSIAN 09 program [57]. Molecular geometries were fully optimized using both the dispersion-corrected-GGA BP86+D [58, 59] and meta-GGA M06-L [59] exchange-correlation functionals. While the former includes the empirical atom-atom dispersion contributions "D" proposed by Grimme [60], the noncovalent forces are taken into account in the latter [21]. Both functionals have been tested by us [23] and found that they provide a suitable description of the olefin metathesis reaction catalyzed by Grubbs catalysts. The ruthenium core electrons were treated by quasi-relativistic effective pseudopotentials (RECPs) developed by Stuttgart group, the so-called MWB28 [61], which replaces the 28 inner electrons by a nonlocal effective potential. The remaining electrons were described with the associated (8s7p6d)/[6s5p3d] basis set. All-electron medium-sized 6-31+$G(d,p)$ basis set was employed for C, H, Cl, P, and N atoms [62]. The harmonic frequency

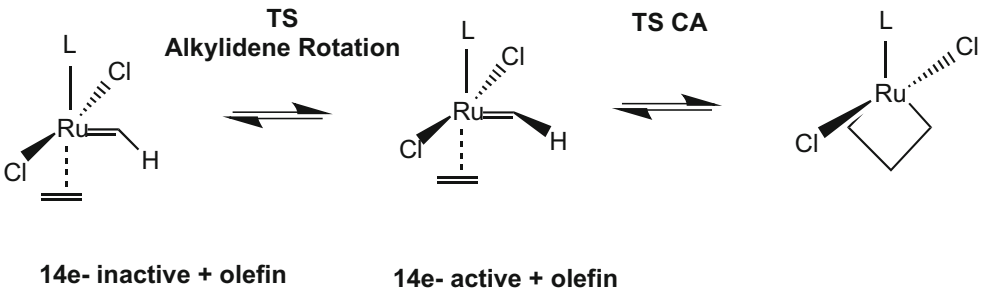

Fig. 4 Alkene coordination, alkylidene rotation, and [2+2] cycloreversion/cycloaddition steps that take place from the 14e- inactive specie. L = PCy_3 (first) and NHC (second generation)

analysis for the stationary points was also carried out using the Hessian matrix in internal coordinates, in order to ensure their nature as minima, intermediate, or transition state on the potential energy surfaces. In addition, we verified the connection between reactants, products, and located transition structures using the intrinsic reaction coordinate (IRC) method [43, 44] only at BP86+D level of theory. This method used a gradient reaction step size of 0.100 $amu^{1/2}$·bohr providing the input $V(\xi)$ profile needed to generate $\mathbf{F}(\xi)$ and $\kappa(\xi)$ reaction profiles, employing the Savitzky-Golay smoothing and differentiation filters for the latter. All electronic structure calculations presented here do not include either solvent or thermal contributions.

Results and discussion

The idea behind the present work was to investigate the alkylidene rotation to transform the 14e- inactive specie into active specie, followed by the [2+2] cycloreversion/cycloaddition using the first- and second-generation Grubbs catalysts (Fig. 4). It was found that, for the first generation, the alkylidene rotation only occurs immediately after the phosphine dissociation. Therefore, while we only studied the Ru-centered [2+2] cycloaddition for the first generation (first-Ru-[2+2] cycloreversion/cycloaddition), both processes, the alkylidene rotation and second-Ru-[2+2] cycloreversion/cycloaddition, are studied for the second-generation Grubbs catalysts.

The profiles of $V(\xi)$, $\mathbf{F}(\xi)$, and $\kappa(\xi)$ along ξ for the Ru-centered [2+2] cycloreversion/cycloaddition, employing the first- and second-generation Grubbs catalysts (first Ru-[2+2] cycloreversion/cycloaddition and second Ru-[2+2] cycloreversion/cycloaddition), are shown in Fig. 5.

The values of energy barriers of 7.6 and 11.0 kcal mol^{-1} are extracted from $V(\xi)$ for the first- and second-Ru-[2+2] cycloreversion/cycloaddition, respectively, with the former being more feasible from a kinetic viewpoint, presenting an enhanced reactivity by almost 10^4 times at 186 K. Accordingly, Ru-centered [2+2] cycloaddition is thus an isoenergetic process. The $\mathbf{F}(\xi)$ profile allows identifying five key points along ξ. Their structures are shown in Fig. 6. Some bond lengths and dihedral angle involved in the coordination sphere of the complexes are quoted in Table 1.

Notice that $\mathbf{F}(\xi)$ is negative in the reactant region is resisting to structural changes, and concomitantly, retarding the process. However, after ξ_1, $\mathbf{F}(\xi)$ suffers a positive increase, reaching a maximum at ξ_2, supporting the transformation and the system starts to relax until the product is reached at ξ_p. It is found that the bonds labeled as **2** and **4** (H_2**C-C(1)** and **Ru-C(2)**H_2, respectively) are stretched from ξ_R to ξ_{TS}. They are shortened when the ruthenacyclobutane intermediate is formed again, i.e., from ξ_{TS} to ξ_P. The breaking/forming of two single bonds (Ru-C and C-C) is mainly encompassed throughout the whole transition region, i.e., from ξ_1 to ξ_2. Likewise, the bonds labeled as **1** and **3** (**Ru=C**H_2 and H_2**C(2)=C(1)**H_2, respectively) undergo significant changes, as result of sp^3 hybridization C atoms which are transforming into sp^2 at the TS. However, these changes mainly take place from ξ_R to ξ_1. Afterward, such changes are slight, in accordance with their double-bond character at the TS. Finally, the dihedral angles **P-Ru=CH** (**C-Ru=CH**) show that movements of the active form occur near to 90°. Specifically, in the transition state, the **P-Ru=CH** (**C-Ru=CH**) angles are 101.67° (99.37°) while in the respective ruthenacyclobutanes are at angles of 71.87° (67.03°). This indicates the importance of the freedom degree in the Ru-centered [2+2] cycloreversion/cycloaddition.

From Table 1, it must be noted that the structural changes are greater in the first generation than in the second generation. However, the partition of the energy barrier into its contributions, quoted in Table 2, reveals that the energy amount associated with the structural contributions are higher in the second-generation Grubbs catalyst than in the first generation, which shows a major rigidity in the ruthenacyclobutanes with NHC ligand. By taking into account that the Ru-centered [2+2] cycloreversion do not present exclusively structural or electronics effects in the reactant region, ξ_R to ξ_1, and the transition region, ξ_1 to ξ_2, respectively. This suggests that in the second generation some stronger electronic effects are involved than in the first generation, related with the donor/acceptor nature of the NHC ligand [63] and the unique donor nature of the phosphine ligand [64].

The results associated with the partitioning of the activation energies ΔE_{act} to the Ru-centered [2+2] cycloreversion/

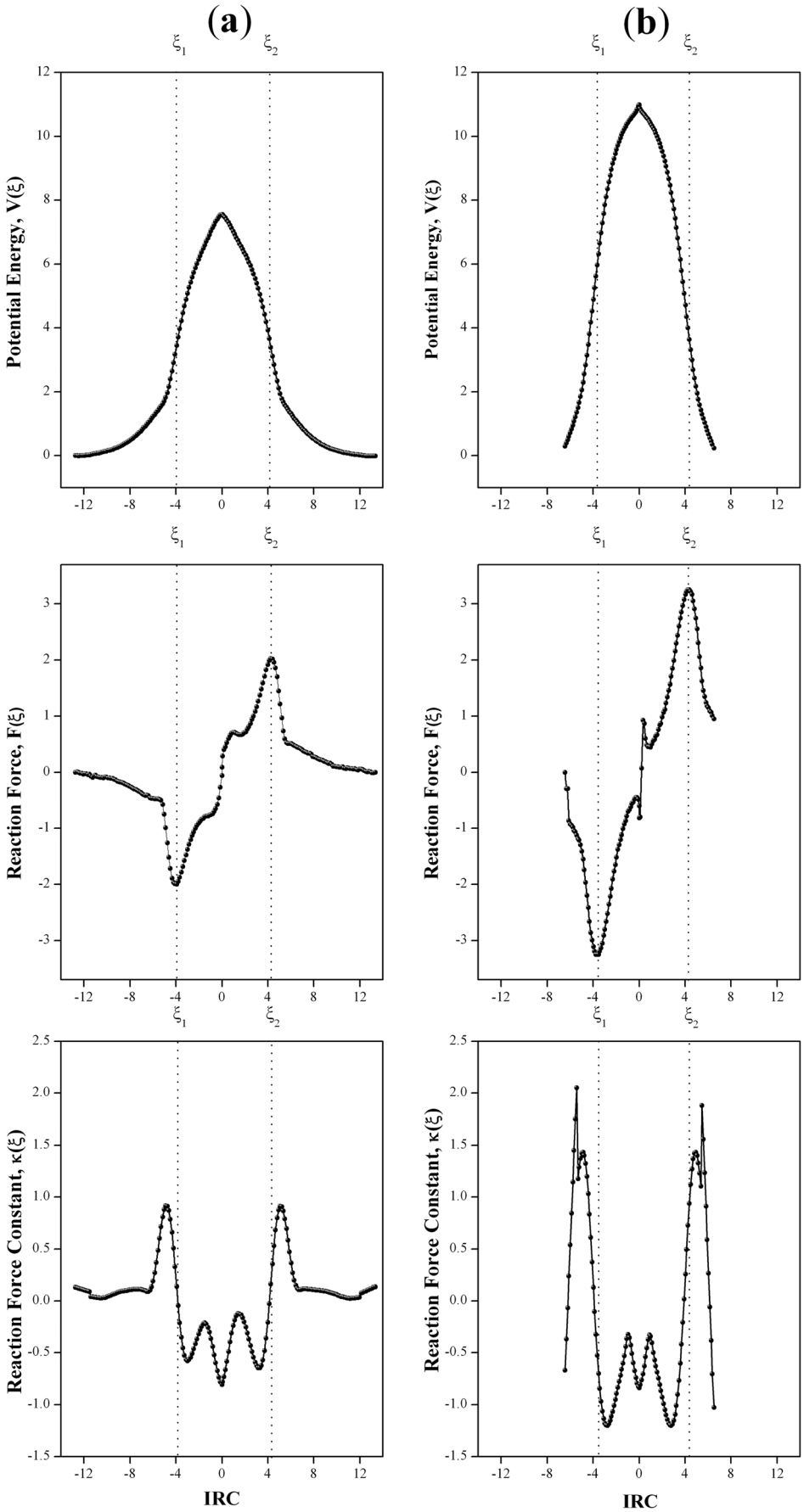

Fig. 5 Profile of $V(\xi)$, $\mathbf{F}(\xi)$, and $\kappa(\xi)$ along ξ for [2+2] cycloreversion/cycloadditions using **a** first- and **b** second-generation Grubbs catalysts

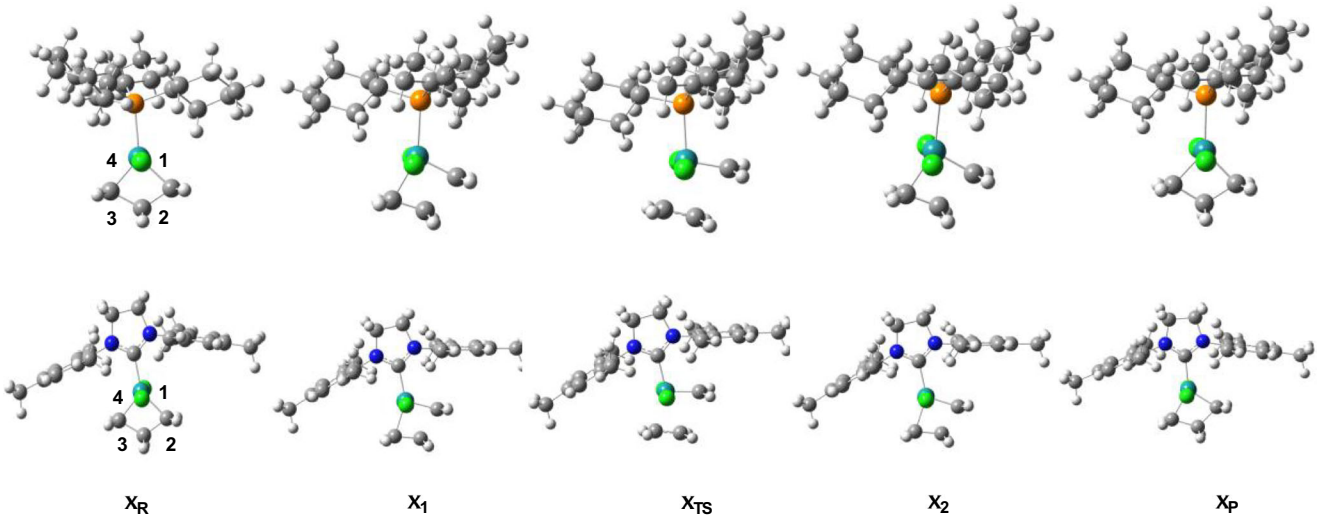

Fig. 6 The five key structures along ξ for the Ru-centered [2+2] cycloreversion/cycloadditions using the first- and second-generation Grubbs catalysts

cycloaddition through of the reaction force indicating that in both generations of Grubbs catalysts, $\Delta E_{act,\,1}$ is higher than the $\Delta E_{act,\,2}$, representing almost the 60 % and 40 % of the overall energy barrier, respectively, although these percentages are slightly lower and higher for the second generation than for the first generation. These findings are in agreement with others computational results, which indicate that the second generation is driven mainly by electronic effects [24], where a minor structural reorganization takes place in the initial steps into of the catalytic cycle of the olefin metathesis [23, 28].

Table 1 Bond distances (in Å) and dihedral angle (in degree) at the key points along ξ for the Ru-centered [2+2] cycloreversion/cycloadditions using the first- and second-generation Grubbs catalysts. The bond labels are in Fig. 5

	ξ_R	ξ_1	ξ_{TS}	ξ_2	ξ_P
First generation					
1. Ru=CH_2	1.985	1.867	1.830	1.866	1.959
2. H_2**C-C(1)**	1.579	1.941	2.493	1.939	1.604
3. H_2**C(2)=C(1)**H_2	1.603	1.466	1.395	1.463	1.579
4. Ru-C(2)H_2	1.959	2.109	2.252	2.114	1.985
(R_3)**P-Ru=C(H)**	71.87	82.50	101.67	82.91	69.21
Second generation					
1. Ru=CH_2	1.952	1.872	1.833	1.890	1.950
2. H_2**C-C(1)**	1.607	1.908	2.493	1.777	1.608
3. H_2**C(2)=C(1)**H_2	1.577	1.476	1.394	1.508	1.575
4. Ru-C(2)H_2	1.997	2.100	2.252	2.068	1.999
(NH)**C-Ru=C(H)**	67.03	70.99	99.37	75.94	69.44

Also, we computed the relative rate constants at 186 K, confirming that the enhanced reactivity for the first generation in Ru-centered [2+2] cycloreversion/cycloaddition is mainly controlled by structural factors, rather than by electronic component.

On the other hand, in the analysis of the reaction force constant $\kappa(\xi)$, in the bottom panels in Fig. 5, we observe that $\kappa(\xi)$ is positive in the reactants and product regions, and negative in the transition region, showing three $\kappa(\xi)$ minima connected by two negative $\kappa(\xi)$ maxima in the region defined between ξ_1 and ξ_2. This peculiar behavior combined with the fact of the barrier width, it can thus be classified as a "two-stage"-concerted reaction in both cases, i.e., for the first- and second-Ru-centered [2+2] cycloreversion/cycloaddition reactions. These reactions reveal a high degree of asynchronicity in such processes, which is slightly higher in the first-Ru-centered [2+2] cycloreversion/cycloaddition. This, in turn, explains its kinetically feasibility.

Regarding the alkylidene rotation in the second-generation Grubbs catalyst, we also analyze the $V(\xi)$, $\mathbf{F}(\xi)$, and $\kappa(\xi)$ profiles, as displayed in Fig. 7. $V(\xi)$ shows that the interconversion of ruthenacyclobutanes advances overcoming an

Table 2 Activation energy, ΔE_{act}, and its components, $\Delta E_{act,\,1}$ and $\Delta E_{act,\,2}$, for the Ru-centered [2+2] cycloreversion/cycloaddition using first- and second-generation Grubbs catalysts (in kcal mol^{-1}) and relative rate constants k_{rel}

Grubbs catalysts	ΔE_{act}	$\Delta E_{act,\,1}$	$\Delta E_{act,\,2}$	k_{rel}	$k_{struct,\,rel}$	$k_{electr,\,rel}$
First generation	7.6	4.5 (59.2 %)	3.1 (40.8 %)	9.9×10^3	1.3×10^2	76
Second generation	11.0	6.3 (57.3 %)	4.7 (42.7 %)	1	1	1

Relative rate constants are computed at 186 K as $k_{rel} = e^{-\Delta\Delta E_{act}/RT}$

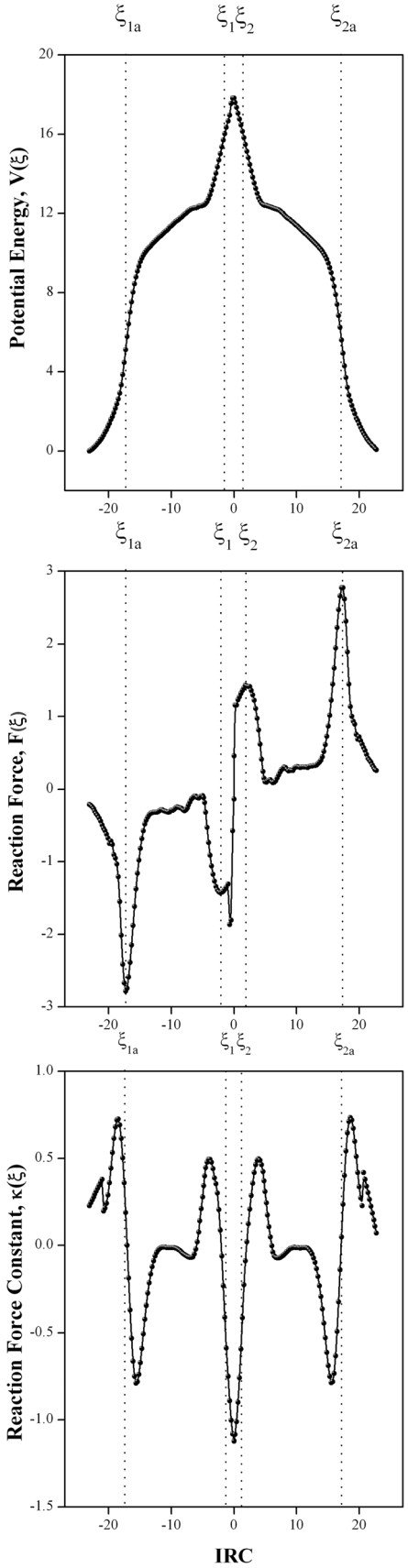

Fig. 7 Profile of $V(\xi)$, $\mathbf{F}(\xi)$, and $\kappa(\xi)$ along ξ alkylidene rotation using the second-generation Grubbs

activation barrier of 17.8 kcal mol^{-1} via the alkylidene rotation path. This is an agreement with other previously reported experimental and computational values, confirming that the [2+2] cycloreversion/cycloaddition mode occurs in the ruthenacycles exchange [22, 29]. Furthermore, this less favorable path exhibits the presence of several transient states, which were identified from the reaction force analysis. These key points along ξ are depictured in Fig. 8. ξ_{1a} defines the transition region of [2+2] cycloreversion/cycloaddition step (ξ_{TS} in Fig. 5), ξ_1 defines the transition region of the alkene coordination involving the 14e- inactive specie and the olefin.

Therefore, "two reactant regions" are noted in the coupled pathway to the alkylidene rotation: from ξ_R to ξ_{1a}, involve the preparation of a [2+2] cycloreversion, while from ξ_{1a} to ξ_1, in which the carbene rotation C-Ru=CH occurs. After, the "transition region," ξ_1 to ξ_2, involves the formation of the transition structure, ξ_{TS}. Finally, "two products regions" also occur, giving rise to the formation of a new ruthenacyclobutane intermediate.

Table 3 contains the four most important bond distances (**1**-Ru=CH_2, **2**-H_2C-C(1), **3**-$H_2C(2)$=C(1)H_2, and **4**-Ru-C(2)H_2) on each one of the identified species along the reaction pathway identified as key points. The results show that in the reactant region, i.e., ξ_R to ξ_{1a}, the bonds labeled as **2** and **4** are stretched as a consequence of the bond-breaking in the ruthenacyclobutanes, as part of the [2+2] cycloreversion and alkylidene rotation that are occurring. In the next reactive region, ξ_{1a} to ξ_1, the most prominent change is the rotation of the dihedral angle C-Ru=CH from 90.50° in ξ_{1a} to −176.21° in ξ_1, passing from an active form to an inactive one. In the "transition region," it is important to highlight that the bonds labeled as **2** and **4** continuously stretch while the olefin and 14e-Ru-methylidene specie move apart when the C-Ru=CH dihedral angle rotates. Finally, the opposite behavior in the "two products regions" occurs, since the intermediate specie come back to the active form (88.32°) in ξ_2 to ξ_{2a} occurring after the [2+2] cycloaddition in ξ_{2a} to ξ_P.

Insights into the reaction from $\mathbf{F}(\xi)$ is found a similar behavior to that observed in the [2+2] cycloreversion/cycloaddition previously studied. $\mathbf{F}(\xi)$ is negative in the reactant region and positive in the product region. Nevertheless, one additional minimum in the first region and one additional maximum in the last region were found as a consequence of the two primitive processes that occur before and after the transition region, respectively. These also show that more changes must be overcome to achieve the barrier energy, which is higher than in the previous processes studied. Within the reaction force frame, the structural alterations are dominant in the reactant and product regions, while the electronic changes, in the transition region. This can be quantified by the amount of energy given by eqn. (3); it is found that the energetic contributions are 9.5, 3.2, and 5.1 kcal mol^{-1}, respectively, for $\Delta E_{act,\ 1}$, $\Delta E_{act,\ 1a}$, and $\Delta E_{act,\ 2}$. Accordingly,

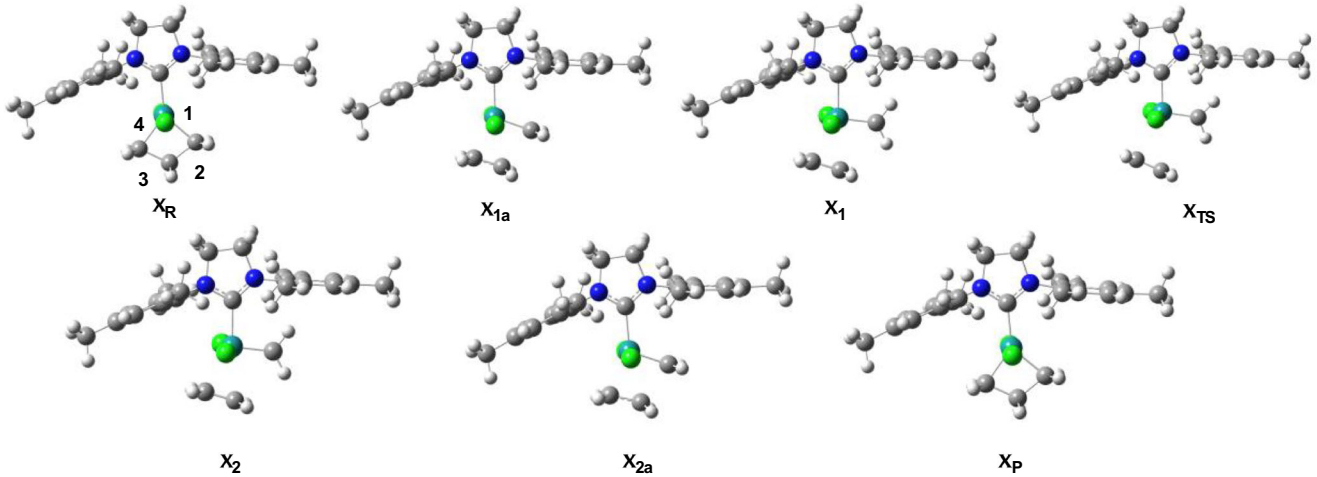

Fig. 8 The key structures along ξ for the alkylidene rotation Ru-centered [2+2] cycloreversion/cycloadditions using the second-generation Grubbs catalyst

Table 3 Bond distances (in Å) and dihedral angles (in degree) at the key points along the reaction pathways for the alkylidene rotation using the second-generation Grubbs catalysts. The bond labels are in Fig. 8

Second generation	ξ_R	ξ_{1a}	ξ_1	ξ_{TS}	ξ_2	ξ_{2a}	ξ_P
1. Ru=CH_2	1.971	1.845	1.832	1.821	1.833	1.854	1.969
2. H_2**C-C(1)** (olefin)	1.594	2.233	2.809	3.245	2.752	2.098	1.594
3. H_2**C(2)=C(1)**H_2	1.588	1.419	1.374	1.357	1.378	1.439	1.587
4. Ru-C(2)H_2	1.978	2.182	2.384	2.713	2.332	2.146	1.980
C-Ru=CH	72.37	90.50	− 177.15	− 176.21	− 179.31	88.32	72.42

the barrier energy to the alkylidene rotation mechanism can be understood as the sum of the barrier energy associated with the [2+2] cycloreversion (9.5 kcal mol^{-1}), plus the energy barrier of the rotation itself (8.3 kcal mol^{-1}), although this amount of energy contains some information related to [2+2] cycloreversion. Again, it is noted that the rate constant is rather controlled by a structural component than an electronic component.

Finally, the reaction force constant $\kappa(\xi)$ analysis showed that it is also very similar to what is described in Fig. 5. This is slightly positive in the reactants and product regions, and negative throughout whole the transition region. Therefore, the alkylidene rotation certainly evidenced sequential primitive processes; however, the pattern noted for [2+2] cycloreversion (cycloaddition), between ξ_R and ξ_{1a} (ξ_{2a} and ξ_P), is nearly asynchronous, and consequently, this fact could explain the higher energy barrier for this mechanism.

Conclusions

The analysis of reaction force and reaction force constant in Ru-centered [2+2] cycloreversion/cycloaddition and alkylidene rotations as paths to interconvert ruthenacyclobutane intermediates employing both the first- and second-generations Grubbs catalysts was carried out. In the first case, the reactant region encompasses the breaking of single Ru-C and C-C bonds in favor of the formation of double-bond character, Ru=C and C=C, at the transition state. The reaction force allows the partitioning of the energy barrier into two components, a structural and an electronic one, and concomitantly, the respective rate constants. The results showed that the [2+2] cycloreversion is mainly controlled by structural factors in both Grubbs catalysts, being more kinetically favorable using the first generation than the second generation. Despite noting minor structural changes in the second generation, the energetic contributions are larger than in the first generation, which agrees with rigidity and the donor/acceptor properties of the NHC ligand. On the basis of the reaction force constant, both processes can be classified as "two-stage"-concerted reactions, unveiling properly a fine structure of $\kappa(\xi)$ along the transition region with two $\kappa(\xi)$ maxima connected by a minimum.

On the other hand, the alkylidene rotation in the second generation was shown to be a less favorable process to interconvert ruthenacyclobutanes than the above pathways. The reaction force revealed that [2+2] cycloreversion and alkylidene torsion are primitive processes occurring in a sequential fashion, its energy barrier is, again, controlled by structural component. $\kappa(\xi)$ displayed that the [2+2] cycloreversion is less asynchronous than in the first case.

Acknowledgments K.P-G., F.M, and P.J thank CONICYT through the FONDECYT projects 3170117, 1180158, and 1181914, respectively. Moreover, K.P-G. acknowledges "CONICYT+PAI+CONVOCATORIA NACIONAL SUBVENCIÓN A INSTALACIÓN EN LA ACADEMIA CONVOCATORIA AÑO 2018 + PAI77180024."

References

1. Grubbs RH, Wenzel AG (2015) Handbook of metathesis, volume 1: catalyst development and mechanism. WILEY-VCH, Weinheim, Germany
2. Feng K, Xie N, Chen B et al (2016) Modular design of poly(norbornenes) for organelle-specific imaging in tumor cells. Biomacromolecules 17:538–545. https://doi.org/10.1021/acs.biomac.5b01450
3. Hughes DL (2016) Highlights of the recent U.S. patent literature: focus on metathesis. Org Process Res Dev 20:1008–1015. https://doi.org/10.1021/acs.oprd.6b00167
4. Sinclair F, Alkattan M, Prunet J, Shaver MP (2017) Olefin cross metathesis and ring-closing metathesis in polymer chemistry. Polym Chem 8:3385–3398. https://doi.org/10.1039/c7py00340d
5. Liu P, Ai C (2018) Olefin metathesis reaction in rubber chemistry and industry and beyond. Ind Eng Chem Res 57:3807–3820. https://doi.org/10.1021/acs.iecr.7b03830
6. Mcconville DH, Wolf JR, Schrock RR (1993) Synthesis of chiral molybdenum ROMP initiators and all-cis highly tactic poly(2,3-(R)2norbornadiene) (R= CF3 or CO2Me). J Am Chem Soc 115:4413–4414. https://doi.org/10.1021/ja00063a090
7. Schrock RR (2006) Multiple metal-carbon bonds for catalytic metathesis reactions (Nobel lecture). Angew Chem Int Ed Eng 45:3748–3759. https://doi.org/10.1002/anie.200600085
8. Singh R, Schrock RR, Müller P, Hoveyda AH (2007) Synthesis of monoalkoxide monopyrrolyl complexes Mo(NR)(CHR′) (OR″)(pyrrolyl): Enyne metathesis with high oxidation state catalysts. J Am Chem Soc 129:12654–12655. https://doi.org/10.1021/ja075569f
9. Samojłowicz C, Bieniek M, Grela K (2009) Ruthenium-based olefin metathesis catalysts bearing N-heterocyclic carbene ligands. Chem Rev 109:3708–3742. https://doi.org/10.1021/cr800524f
10. Vougioukalakis GC, Grubbs RH (2010) Ruthenium-based heterocyclic carbene-coordinated olefin metathesis catalysts. Chem Rev 110:1746–1787. https://doi.org/10.1021/cr9002424
11. Schwab P, Grubbs RH, Ziller JW, August RV (1996) Synthesis and applications of RuCl2 (=CHR′)(PR3)2 : the influence of the alkylidene moiety on metathesis activity. J Am Chem Soc 118:100–110. https://doi.org/10.1021/ja952676d
12. Scholl M, Ding S, Lee CW, Grubbs RH (1999) Synthesis and activity of a new generation of ruthenium-based olefin metathesis catalysts coordinated with 1,3-dimesityl-4,5-dihydroimidazol-2-ylidene ligands. Org Lett 1:953–956. https://doi.org/10.1021/ol990909q
13. Huang J, Stevens ED, Nolan SP et al (1999) Olefin metathesis-active ruthenium complexes bearing a nucleophilic carbene ligand. J Am Chem Soc 121:2674–2678. https://doi.org/10.1021/ja9831352
14. Keitz BK, Endo K, Patel PR et al (2012) Improved ruthenium catalysts for Z-selective olefin metathesis. J Am Chem Soc 134:693–699. https://doi.org/10.1021/ja210225e
15. Khan RKM, Torker S, Hoveyda AH (2014) Reactivity and selectivity differences between catecholate and catechothiolate ru complexes. Implications regarding design of stereoselective olefin metathesis catalysts. J Am Chem Soc 136:14337–14340. https://doi.org/10.1021/ja505961z
16. Herisson PJ-L, Chauvin Y (1970) Catalyse de transformation des olefines par les complexes du tugstene. Macromol Chem Phys:161–176. https://doi.org/10.1002/macp.1971.021410112
17. Chauvin Y (2006) Olefin metathesis: the early days (Nobel lecture). Angew Chem Int Ed Eng 45:3740–3747. https://doi.org/10.1002/anie.200601234
18. Cavallo L (2002) Mechanism of ruthenium-catalyzed olefin metathesis reactions from a theoretical perspective. J Am Chem Soc 124:8965–8973. https://doi.org/10.1021/ja016772s
19. Tsipis AC, Orpen a G, Harvey JN (2005) Substituent effects and the mechanism of alkene metathesis catalyzed by ruthenium dichloride catalysts. Dalton Trans:2849–2858. https://doi.org/10.1039/b506929g
20. Torker S, Merki D, Chen P (2008) Gas-phase thermochemistry of ruthenium carbene metathesis catalysts. J Am Chem Soc 130:4808–4814. https://doi.org/10.1021/ja078149z
21. Zhao Y, Truhlar DG (2007) Attractive noncovalent interactions in the mechanism of grubbs second-generation Ru catalysts for olefin metathesis. Org Lett 9:1967–1970. https://doi.org/10.1021/ol0705548
22. Paredes-Gil K, Solans-Monfort X, Rodriguez-Santiago L et al (2014) DFT study on the relative stabilities of substituted ruthenacyclobutane intermediates involved in olefin cross-metathesis reactions and their interconversion pathways. Organometallics 33:6065–6075. https://doi.org/10.1021/om500718a
23. Paredes-Gil K, Jaque P (2016) Theoretical characterization of first and second generation Grubbs catalysts in styrene cross-metathesis reactions: insights from conceptual DFT. Catal Sci Technol 6:755–766. https://doi.org/10.1039/c5cy00826c
24. Paredes-Gil K, Jaque P (2015) Initiation stage of alkene metathesis: insights from natural bond orbital and charge decomposition analyses. Chem Phys Lett 608:174–181. https://doi.org/10.1016/j.cplett.2014.11.007
25. Sanford MS, Love JA, Grubbs RH (2001) A versatile precursor for the synthesis of new ruthenium olefin metathesis catalysts. Organometallics:5314–5318
26. Sanford MS, Ulman M, Grubbs RH (2001) New insights into the mechanism of ruthenium-catalyzed olefin metathesis reactions. J Am Chem Soc 123:749–750. https://doi.org/10.1021/ja003582t
27. Minenkov Y, Occhipinti G, Heyndrickx W, Jensen VR (2012) The nature of the barrier to phosphane dissociation from Grubbs olefin metathesis catalysts. Eur J Inorg Chem 2012:1507–1516. https://doi.org/10.1002/ejic.201100932
28. Yang H-C, Huang Y-C, Lan Y-K et al (2011) Carbene rotamer switching explains the reverse trans effect in forming the Grubbs second-generation olefin metathesis catalyst. Organometallics 30:4196–4200. https://doi.org/10.1021/om200529m
29. Wenzel AG, Blake G, VanderVelde DG, Grubbs RH (2011) Characterization and dynamics of substituted ruthenacyclobutanes relevant to the olefin cross-metathesis reaction. J Am Chem Soc 133:6429–6439. https://doi.org/10.1021/ja2009746
30. Wenzel AG, Grubbs RH (2006) Ruthenium metallacycles derived from 14-electron complexes. New insights into olefin metathesis intermediates. J Am Chem Soc 128:16048–16049. https://doi.org/10.1021/ja0666598
31. Toro-Labbé A (1999) Characterization of chemical reactions from the profiles of energy, chemical potential, and hardness. J Phys Chem A 103:4398–4403. https://doi.org/10.1021/jp984187g
32. Politzer P, Toro-Labbé A, Gutiérrez-Oliva S, Murray JS (2012) Perspectives on the reaction force. In: Sabin JR BE (eds) (ed) Advances in quantum chemistry. pp 189–209
33. Jaque P, Toro-Labbé A, Politzer P, Geerlings P (2008) Reaction force constant and projected force constants of vibrational modes

along the path of an intramolecular proton transfer reaction. Chem Phys Lett 456:135–140. https://doi.org/10.1016/j.cplett.2008.03.054
34. Politzer P, Murray JS, Jaque P (2013) Perspectives on the reaction force constant. J Mol Model 19:4111–4118. https://doi.org/10.1007/s00894-012-1713-8
35. Smith MW, Baran PS (2015) As simple as [2+2]. Science (80-) 349:925–926. https://doi.org/10.1126/science.aac9883
36. Dewar MJS (1984) Multibond reactions cannot normally be synchronous. J Am Chem Soc 106:209–219. https://doi.org/10.1021/ja00313a042
37. Yepes D, Murray JS, Santos JC et al (2013) Fine structure in the transition region: reaction force analyses of water-assisted proton transfers. J Mol Model 19:2689–2697. https://doi.org/10.1007/s00894-012-1475-3
38. Yepes D, Murray JS, Politzer P, Jaque P (2012) The reaction force constant: an indicator of the synchronicity in double proton transfer reactions. Phys Chem Chem Phys 14:11125–11134. https://doi.org/10.1039/c2cp41064h
39. Yepes D, Donoso-Tauda O, Pérez P et al (2013) The reaction force constant as an indicator of synchronicity/nonsynchronicity in [4+2] cycloaddition processes. Phys Chem Chem Phys 15:7311–7320. https://doi.org/10.1039/c3cp44197k
40. Yepes D, Murray JS, Pérez P et al (2014) Complementarity of reaction force and electron localization function analyses of asynchronicity in bond formation in Diels-Alder reactions. Phys Chem Chem Phys 16:6726–6734. https://doi.org/10.1039/c3cp54766c
41. Murray JS, Yepes D, Jaque P, Politzer P (2015) Insights into some Diels-Alder cycloadditions via the electrostatic potential and the reaction force constant. Comput Theor Chem 1053:270–280. https://doi.org/10.1016/j.comptc.2014.08.010
42. Yepes D, Valenzuela J, Martínez-Araya JI et al (2019) Effect of the exchange-correlation functional on the synchronicity/nonsynchronicity in bond formation in Diels-Alder reactions: a reaction force constant analysis. Phys Chem Chem Phys 21:7412–7428. https://doi.org/10.1039/c8cp02284d
43. Fukui K (1981) The path of chemical reactions - the IRC approach. Acc Chem Res 14:363–368. https://doi.org/10.1021/ar00072a001
44. Gonzalez C, Schlegel HB (1990) Reaction path following in mass-weighted internal coordinates. J Phys Chem 94:5523–5527. https://doi.org/10.1021/j100377a021
45. Jaque P, Toro-Labbé A (2000) Theoretical study of the double proton transfer in the CHX-XH ⋯ CHX-XH (X = O, S) complexes. J Phys Chem A 104:995–1003. https://doi.org/10.1021/jp993016o
46. Martínez J, Toro-Labbé A (2009) The reaction force. A scalar property to characterize reaction mechanisms. J Math Chem 45:911–927. https://doi.org/10.1007/s10910-008-9478-0
47. Toro-Labbé A, Gutiérrez-Oliva S, Concha MC et al (2004) Analysis of two intramolecular proton transfer processes in terms of the reaction force. J Chem Phys 121:4570–4576. https://doi.org/10.1063/1.1777216
48. Gutiérrez-Oliva S, Herrera B, Toro-Labbé A, Chermette H (2005) On the mechanism of hydrogen transfer in the HSCH(O) ⇄ (S)CHOH and HSNO ⇄ SNOH reactions. J Phys Chem A 109:1748–1751. https://doi.org/10.1021/jp0452756
49. Herrera B, Toro-Labbé A (2007) The role of reaction force and chemical potential in characterizing the mechanism of double proton transfer in the adenine-uracil complex. J Phys Chem A 111:5921–5926. https://doi.org/10.1021/jp065951z
50. Jaque P, Toro-Labbe A, Geerlings P, De Proft F (2009) Theoretical study of the regioselectivity of [2 + 2] photocycloaddition reactions of acrolein with olefins. J Phys Chem A 113:332–344. https://doi.org/10.1021/jp807754f
51. Martínez-Araya JI, Quijada R, Toro-labbe A (2012) The mechanism of ethylene polymerization reaction catalyzed by group IVB metallocenes. A rational analysis through the use of reaction force. J Phys Chem C 116:21318–21325. https://doi.org/10.1021/jp302702h
52. Politzer P, Murray JS, Yepes D, Jaque P (2014) Driving and retarding forces in a chemical reaction. J Mol Model 20:2351–2357. https://doi.org/10.1007/s00894-014-2351-0
53. Toro-Labbé A, Gutiérrez-Oliva S, Murray JS, Politzer P (2009) The reaction force and the transition region of a reaction. J Mol Model 15:707–710. https://doi.org/10.1007/s00894-008-0431-8
54. Politzer P, Toro-Labbé A, Gutiérrez-Oliva S et al (2005) The reaction force: three key points along an intrinsic reaction coordinate. J Chem Sci 117:467–472. https://doi.org/10.1007/BF02708350
55. Rincón E, Jaque P, Toro-Labbé A (2006) Reaction force analysis of the effect of Mg(II) on the 1,3 intramolecular hydrogen transfer in thymine. J Phys Chem A 110:9478–9485. https://doi.org/10.1021/jp062870u
56. Burda JV, Toro-Labbé A, Gutiérrez-Oliva S et al (2007) Reaction force decomposition of activation barriers to elucidate solvent effects. J Phys Chem A 111:2455–2457. https://doi.org/10.1021/jp0709353
57. Frisch MJ, Trucks GW, Schlegel HB, Scuseria GE, Robb MA, Cheeseman JR, Scalmani G, Barone V, Petersson GA, Nakatsuji H, Li X, Caricato M, Marenich AV, Bloino J, Janesko BG, Gomperts R, Mennucci B, Hratchian HP, Ortiz JV, Izmaylov AF, Sonnenberg JL W, DJ F (2009) Gaussian 09 Rev. B.01
58. Becke AD (1988) Correlation energy of an inhomogeneous electron gas: a coordinate-space model. J Chem Phys 88:1053–1062. https://doi.org/10.1063/1.454274
59. Zhao Y, Truhlar DG (2006) A new local density functional for main-group thermochemistry, transition metal bonding, thermochemical kinetics, and noncovalent interactions. J Chem Phys 125:194101–194118. https://doi.org/10.1063/1.2370993
60. Grimme S (2004) Accurate description of van der Waals complexes by density functional theory including empirical corrections. J Comput Chem 25:1463–1473. https://doi.org/10.1002/jcc.20078
61. Andrae D, H U, Dolg M et al (1990) Energy-adjusted ab initio pseudopotentials for the second and third row transition elements. Theor Chim Acta 77:123–141. https://doi.org/10.1007/BF01114537
62. Hehre WJ, Ditchfield R, Pople JA (1972) Self—consistent molecular orbital methods. XII. Further extensions of Gaussian—type basis sets for use in molecular orbital studies of organic molecules. J Chem Phys 56:2257–2261. https://doi.org/10.1063/1.1677527
63. Jacobsen H, Correa A, Poater A et al (2009) Understanding the M(NHC) (NHC=N-heterocyclic carbene) bond. Coord Chem Rev 253:687–703. https://doi.org/10.1016/j.ccr.2008.06.006
64. Antonova NS, Carbó JJ, Poblet JM (2009) Quantifying the donor −acceptor properties of phosphine and N-heterocyclic carbene ligands in Grubbs' catalysts using a modified EDA procedure based on orbital deletion. Organometallics 28:4283–4287. https://doi.org/10.1021/om900180m